

Phase Separation, Edge Currents, and Hall Effect for Active Matter with Magnus Dynamics

B. Adorjáni¹, A. Libál¹, C. Reichhardt³, and C. J. O. Reichhardt³

¹ *Mathematics and Computer Science Department, Babeş-Bolyai University, Cluj 400084, Romania*

² *Theoretical Division and Center for Nonlinear Studies,*

Los Alamos National Laboratory, Los Alamos, New Mexico 87545, USA

(Dated: October 27, 2023)

We examine run and tumble disks in two-dimensional systems where the particles also have a Magnus component to their dynamics. For increased activity, we find that the system forms a motility-induced phase-separated (MIPS) state with chiral edge flow around the clusters, where the direction of the current is correlated with the sign of the Magnus term. The stability of the MIPS state is non-monotonic as a function of increasing Magnus term amplitude, with the MIPS region first extending down to lower activities followed by a break up of MIPS at large Magnus amplitudes into a gel-like state. We examine the dynamics in the presence of quenched disorder and a uniform drive, and find that the bulk flow exhibits a drive-dependent Hall angle. This is a result of the side jump effect produced by scattering from the pinning sites, and is similar to the behavior found for skyrmions in chiral magnets with quenched disorder.

I. INTRODUCTION

There is growing interest in active matter systems or systems where some form of self-motility occurs, which are relevant in soft matter, robotic, and biological settings [1]. One of the most well-known effects observed in collections of interacting active particles is motility-induced phase separation (MIPS) [2–7]. Here, even repulsive disks that would form a uniform fluid in thermal equilibrium instead assemble into an active solid that coexists with a low density active liquid. Recent work on active matter systems has increasingly focused on how active matter behaves when coupled to a complex environment, such as confinement, mixtures of active and inactive particles, or a disordered substrate that can enhance or disrupt the MIPS clustering depending on the substrate interaction strength. [8–13]. Different types of trapping effects can also arise [14, 15]. When active matter interacting with a disordered landscape is subjected to bulk driving, depinning phenomena can occur similar to that found for driven passive particles interacting with random disorder. In some cases, increasing the activity can reduce the net mobility through the system due to the enhancement of self-trapping by the activity [16].

Most active matter systems obey overdamped dynamics; however, if additional chiral dynamics are present, such as due to the spinning of the particles, a non-dissipative Magnus term arises. The Magnus term generates a velocity component perpendicular to the net forces experienced by the particle, and Magnus effects appear for fluid vortices [17, 18], magnetic vortices [19], charges in a magnetic field [20, 21], fracton phases [22], and skyrmion textures in chiral magnets [23–26]. Particles with a Magnus term that are subjected to uniform driving move at a Hall angle θ_H with respect to the driving direction, and θ_H increases as the Magnus term becomes larger. Magnus-induced Hall angles similar to the Hall effect found for charges moving in a magnetic field [27] have been observed in simulations [26, 28, 29] and exper-

iments [30, 31] for skyrmions in chiral magnets. The size of the Hall angle at low drives is reduced in the presence of quenched disorder due to a side jump effect in which particles are scattered sideways as they cross a pinning site, but for high drives this scattering is reduced and the Hall angle approaches its intrinsic substrate-free value [26, 28, 30, 31].

Magnus effects can arise in active matter systems when the particles have a chiral shape [32] or are undergoing spinning or circular motion [33–37]. Chiral active colloids have been shown to produce edge currents and odd viscosity effects [38–46], while other studies have demonstrated that chirality can increase the frequency of scattering events and thus increase the diffusive motion of the particles [47]. Recently, Cao *et al.* produced an experimental realization of spinning colloids in viscoelastic fluids that generated very strong Magnus forces and a pronounced Hall angle [48]. For individual particles driven through chiral fluids, a drive dependent Hall angle has been observed [49], and it was also shown that in some cases, a velocity boost effect occurs in which the velocity increases due to the conversion of some of the rotational velocity into translational velocity by the Magnus term [50, 51]. Chiral active matter has also been shown to form large rotating crystals [52–54] and to exhibit wave propagation due to odd viscosity effects [54]. Biological systems often involve chiral active matter, such as in the chiral motion of bacteria [55] or the formation of bacterial vortex lattices [56, 57].

Here we explore how the behavior of active matter changes when a Magnus term is added to the equations of motion. We find that in the MIPS regime, a system with finite Magnus forces forms a rigidly rotating crystalline cluster surrounded by a fast-moving circulating edge current of particles. As the Magnus force increases, the edge current region develops additional shear bands and contains multiple rows of particles moving at different velocities. We also find that the Magnus term stabilizes the MIPS clusters down to lower running lengths compared

to Magnus-free systems. This occurs because forces directed radially away from the cluster, which ordinarily would tend to break the cluster apart, are rotated by the Magnus term into the direction perpendicular to the cluster edge, establishing an edge current and keeping the particles localized at the cluster. For very strong Magnus forces, the clusters break up into chiral labyrinthine states. We examine the dynamics when a random pinning landscape and a drift force are introduced. In the absence of quenched disorder, the clusters move at a constant Hall angle with respect to the direction of the drift force; however, when quenched disorder is present, the Hall angle develops a drive dependence, rising from a low value at low drives before eventually approaching the disorder-free value at high drives. This drive dependence of the Hall angle occurs due to the Magnus-induced asymmetric scattering of active particles by the pinning sites, which is strongest at the lowest drives and decreases for higher drives when the particles spend less time interacting with any given pinning site. A similar drive-dependent Hall angle for motion over quenched disorder has been observed for magnetic skyrmions, which also have a strong Magnus term in their dynamics. We find that the MIPS cluster breaks apart when the disorder is strong, but that the cluster can partially reform at higher drives when the particles are moving sufficiently rapidly that the pinning effectiveness is reduced. We also show that a drive-dependent Hall angle can occur for particles with a Magnus term but no activity. Our results should be relevant to chiral active matter systems and systems with odd viscosity.

II. SIMULATION

We model a two-dimensional system of size $L \times L$ with $L = 160$ that has periodic boundary conditions in both the x and y directions. The sample contains $N = 4000$ circular disks of radius $R_d = 1.0$, giving a particle density of $\phi = N\pi R_d^2/L^2 = 0.49$. Each particle moves under the influence of a motor force $\mathbf{f}_i^{\text{mot}} = F_m \hat{\mathbf{m}}_i$ of magnitude $F_m = 1.0$ applied in a randomly chosen direction $\hat{\mathbf{m}}_i$ during a time interval of τ_i simulation time steps, drawn randomly from the allowed range $\tau_i \in [\tau, 2\tau]$. After τ_i time steps have elapsed, particle i undergoes an instantaneous tumbling event in which new random values of τ_i and $\hat{\mathbf{m}}_i$ are selected. Particles in contact with each other experience a repulsive harmonic potential $\mathbf{f}^{\text{dd}} = f_{\text{dd}} \hat{\mathbf{r}}_{ij}$ with $f_{\text{dd}} = \sum_j^N k(2R_d - r_{ij})\Theta(2R_d - r_{ij})$, where $r_{ij} = |\mathbf{r}_j - \mathbf{r}_i|$ is the distance between particles located at \mathbf{r}_i and \mathbf{r}_j , $\hat{\mathbf{r}}_{ij} = (\mathbf{r}_j - \mathbf{r}_i)/r_{ij}$, Θ is the Heaviside step function, and $k = 20$ is the elastic constant.

The overdamped equation of motion for particle i is

$$\alpha_d \mathbf{v}_i + \omega \hat{\mathbf{z}} \times \mathbf{v}_i = \mathbf{f}_i^{\text{dd}} + \mathbf{f}_i^{\text{mot}} + \mathbf{f}_i^{\text{pin}} + \mathbf{f}^D. \quad (1)$$

where $\mathbf{v}_i = d\mathbf{r}_i/dt$ is the particle velocity. The first term on the left hand side is the damping term

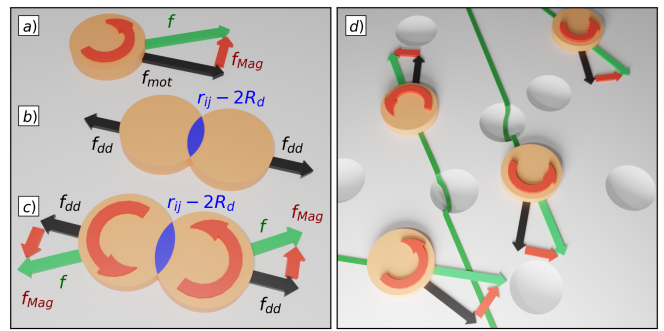


FIG. 1. (a) Schematic of the forces acting on the run-and-tumble Magnus particles (tan disks). The intrinsic propulsion arises from the motor force f^{mot} (black arrow). The Magnus force f^{Mag} (straight red arrow) acts perpendicularly to the net forces on the particle, which in the absence of pinning or particle-particle interactions is only the motor force, giving a final force of f (green arrow). The Magnus force effectively rotates the net forces counterclockwise, as indicated by the circular red arrow. (b) In the absence of the Magnus force, two particles with motor forces directed toward each other (not shown) experience a contact repulsion f^{dd} (black arrows) proportional to the net overlap $r_{ij} - 2R_d$, where R_d is the particle radius. (c) When a Magnus force f^{Mag} (straight red arrow) is added to the particles from panel (b), it produces final forces f (green arrows) that are rotated counterclockwise (circular red arrows). (d) Schematic of an assembly of run-and-tumble Magnus particles (tan disks) interacting with randomly placed non-overlapping pinning sites (divots). Black arrows indicate the instantaneous motor force of each particle, green arrows show the net forces that have been rotated by the Magnus forces (red arrows), and thin green lines illustrate the trajectories of the particles.

of magnitude α_d , while the second term is the Magnus force of magnitude ω , which contributes a velocity component perpendicular to the net force on the particle. Interactions with N_{pin} randomly placed nonoverlapping parabolic pinning sites of radius $R_{\text{pin}} = 0.5$ and maximum strength F_p are given by $\mathbf{f}_i^{\text{pin}} = \sum_k^{N_{\text{pin}}} F_p (r_{ik}^{(p)}/R_{\text{pin}}) \Theta(r_{ik}^{(p)} - R_{\text{pin}}) \hat{\mathbf{r}}_{ik}^{(p)}$, where $r_{ik}^{(p)} = |\mathbf{r}_i - \mathbf{r}_k^{(p)}|$ is the distance between particle i and the pinning site at $\mathbf{r}_k^{(p)}$, and $\hat{\mathbf{r}}_{ik}^{(p)} = (\mathbf{r}_k^{(p)} - \mathbf{r}_i)/r_{ik}^{(p)}$. The final term, $\mathbf{f}^D = F_D \hat{\mathbf{x}}$, represents a uniform drift force applied to all of the particles.

In Fig. 1(a) we show a schematic of the effect of the Magnus term on a freely moving active particle. The Magnus term acts perpendicular to the net applied force, which is only the motor force in this example, and effectively rotates the force counterclockwise, producing a finite Hall angle between the direction of force and the direction of motion. The elastic interaction between two particles with oppositely directed motor forces is illustrated in Fig. 1(b), where the net force pushes the particles directly away from each other. When a Magnus term is added to this interaction, Fig. 1(c) shows that the repulsive forces are effectively rotated counterclock-

wise, causing the particles to be pushed away from each other at an angle to the contact interaction force. In Fig. 1(d) we plot a schematic of the motion of a collection of active Magnus particles driven over randomly placed pinning sites. Upon traversing a pinning site, the particles experience a side slip generated by the Magnus term that reduces the size of the Hall angle. The magnitude of this side slip diminishes as the external drift force F_D increases, causing the Hall angle to approach its intrinsic value at high drives.

To characterize the behavior, we measure the average fraction C_L of particles in the largest cluster, determined using the algorithm described in Ref. [58]. When pinning and a drift force are both present, we also measure the average transport parallel, $\langle V_x \rangle = N^{-1} \sum_i^N \mathbf{v}_i \cdot \hat{\mathbf{x}}$, and perpendicular, $\langle V_y \rangle = N^{-1} \sum_i^N \mathbf{v}_i \cdot \hat{\mathbf{y}}$, to the applied drive. The measured Hall angle is given by $\theta_H = \arctan(\langle V_y \rangle / \langle V_x \rangle)$. In the absence of particle-particle interactions or pinning, the intrinsic Hall angle is $\theta_H^{\text{int}} = \arctan(\omega / \alpha_d)$. We use a simulation time step of size $dt = 0.001$ and allow the system to evolve to a steady state during 2.5×10^6 simulation time steps before collecting data during the next 2.5×10^6 simulation time steps.

III. RESULTS

A. No Quenched Disorder or Drift

We first consider the behavior in the absence of pinning or a drift force in a sample with $\phi = 0.49$ and $\tau = 1.4 \times 10^5$. For these parameters, a MIPS state appears when the Magnus term is absent, $\omega = 0$. Images of the instantaneous particle positions appear in Fig. 2(a-d) for Magnus term magnitudes of $\omega = 1, 2, 6,$ and 10 , respectively. The particles are colored according to their net displacement $\Delta r = |\mathbf{r}_i(t) - \mathbf{r}_i(t - \Delta t)|$ during a time period of $\Delta t = 500$ simulation time steps. For the small but finite Magnus term of $\omega = 1$ in Fig. 2(a), we find a MIPS state where the dense cluster has a net rotation, indicated by an arrow, that is in the same direction as the Magnus force chirality. The rotation is not uniform throughout the cluster; instead, there is a dense nonrotating core surrounded by a rotating halo of particles at the edge of the cluster. The halo particles move from three to eight times faster than particles in the nonrotating core, and as a result, a shear band forms near the cluster edge. For $\omega = 2$ in Fig. 2(b), the rotation speed of the cluster edge has increased and a velocity gradient has developed inside the cluster edge, leading to the appearance of multiple shear band regions. Here, the dense core region of the cluster rotates slowly as a rigid object. The cluster becomes more elongated as the Magnus term increases, and in Fig. 2(c) at $\omega = 6$ the cluster spans the width of the system and develops wide edge regions that are rapidly moving in opposite directions on the top and bottom of the cluster. Here, even though a large dense

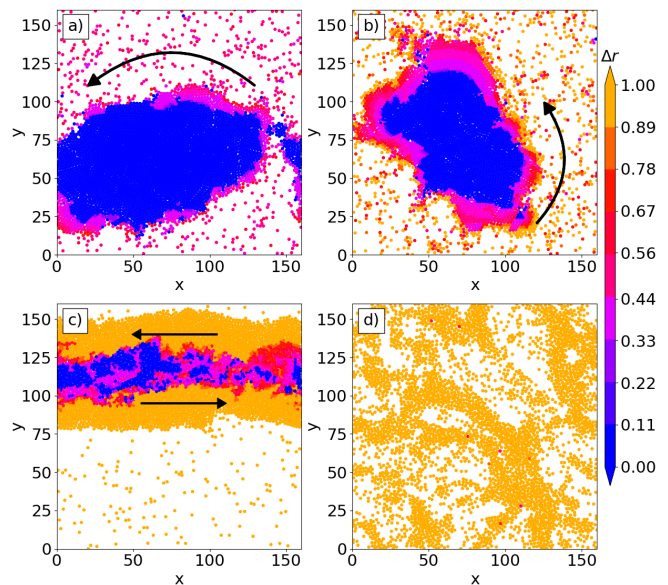


FIG. 2. Images of particle configurations in samples with active Magnus particles and zero drift force, $N_{\text{pin}} = 0$ and $F_D = 0$, at a particle density of $\phi = 0.49$ and a run time $\tau = 1.4 \times 10^5$ for different Magnus term magnitudes of $\omega =$ (a) 1, (b) 2, (c) 6, and (d) 10. Colors indicate the net displacement Δr of the particle during a period of 500 simulation time steps. Arrows indicate the rotation direction of the cluster in panels (a) and (b), and the direction of shear banding flow in panel (c).

cluster still forms, the strong shearing forces destroy the crystalline ordering in the cluster core. When the Magnus term becomes sufficiently large, it interferes with the ability of the particles to nucleate stable clusters due to the force rotation effect illustrated in Fig. 1(c), and the system breaks apart into the clustered fluid state illustrated in Fig. 2(d) for $\omega = 10$.

In Fig. 3(a), we plot the fraction C_L of particles in the largest cluster C_L as a function of ω versus τ for the system from Fig. 2 with $N_{\text{pin}} = 0$ and $F_D = 0$. Dashed squares highlight the values of ω and τ at which the images in Fig. 2 were obtained. When $\omega = 0$, the system forms an ordinary nonrotating MIPS state when τ is sufficiently large, as observed in previous studies [2, 3, 6, 59]. As ω increases to $\omega = 6$, the region where MIPS clusters appears expands by more than a factor of 10 to lower values of τ , indicating that the Magnus term is helping to stabilize the MIPS state. At $\omega = 0$, particles near the cluster edge remain attached to the cluster only as a result of their motor force, which must be aligned in the direction of the cluster in order to prevent a particle from escaping the cluster. When ω is finite, a motor force directed away from the cluster gets rotated and becomes more perpendicular to the cluster edge, causing particles that would have escaped from the cluster to start rotating around the cluster instead, generating an edge current and helping to stabilize the cluster down to lower values of τ . In previous work on driven skyrmions, it was

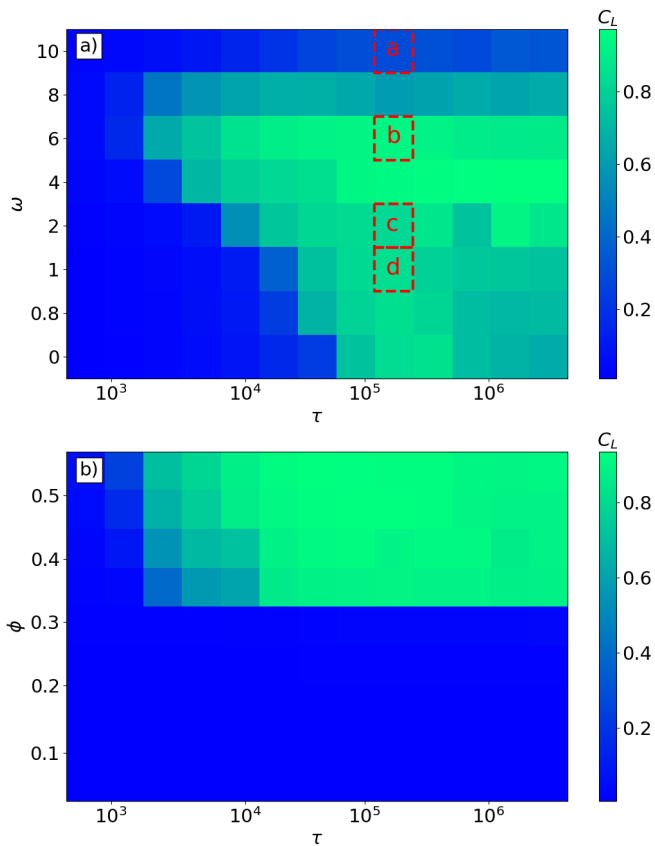


FIG. 3. Heat maps of the fraction C_L of particles in the largest cluster for the system from Fig. 2 with $N_{\text{pin}} = 0$ and $F_D = 0$. (a) C_L as a function of ω vs τ at $\phi = 0.49$. Squares indicate the values of τ and ω at which the images in Fig. 2 were obtained. As ω increases up to $\omega = 6$, the window of τ for which strong clustering occurs becomes wider. Edge currents only appear when $\omega > 0$. (b) C_L as a function of ϕ vs τ at $\omega = 6$ showing that a MIPS state cannot form when $\phi \leq 0.31$.

shown that the Magnus force tended to stabilize skyrmion clusters even though the skyrmion-skyrmion interactions are strictly pairwise repulsive, and that this enhanced clustering originated when the skyrmions tended to spiral around each other instead of moving away from each other [26]. In Fig. 3(b), we plot a heat map of C_L as a function of ϕ versus τ for the same system from Fig. 3(a) at $\omega = 6$. Similar to ordinary MIPS systems with $\omega = 0$, both the activity and the density must be high enough or else the MIPS state does not appear; however, the onset of MIPS occurs at $\tau = 2 \times 10^3$ when $\phi = 0.49$, which is significantly lower than the onset value of $\tau = 7 \times 10^5$ found for $\omega = 0$ in Fig. 3(a). We find in Fig. 3(b) that a MIPS cluster only appears if $\phi > 0.31$.

Our results can be compared to several experiments. In Ref. [38], spinning colloids that form cluster states develop edge currents similar to what we observe. The giant rotating crystal that we find resembles states seen in spinning starfish embryos, which form rigidly rotat-

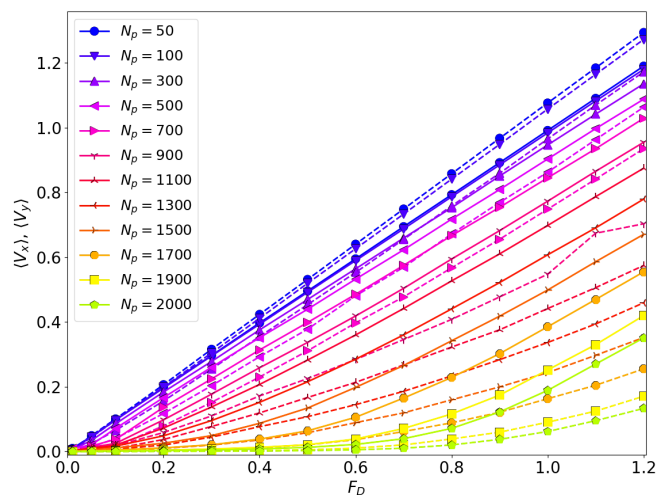


FIG. 4. $\langle V_x \rangle$ (solid lines) and $\langle V_y \rangle$ (dashed lines) vs F_D in a sample with $\omega = 1.1$, $\phi = 0.49$, and $\tau = 1.4 \times 10^5$ at $F_p = 7$ for varied number of pinning sites $N_p = 50, 100, 300, 500, 700, 900, 1100, 1300, 1500, 1700, 1900$, and 2000 , from top to bottom.

ing clusters [54]. Unlike the embryos, which have an intermediate-range attractive component in the particle-particle interactions due to hydrodynamic effects, for our system the rotation is not rigid but instead produces a shear band that separates a rapidly rotating edge region from a more slowly rotating or nonrotating bulk rigid crystal region, as shown in Fig. 2(a,b). The particle-particle interactions in our system are strictly repulsive and the cluster can only be stabilized by the motor force and by the Magnus rotation of the motor force.

B. Quenched Disorder Plus Drift

We next introduce quenched disorder in the form of randomly placed pinning sites and apply a finite drift force F_D . In non-active systems such as skyrmions under the same conditions, the Magnus term causes the particles to move at a finite Hall angle with respect to the drift direction. In Fig. 4 we plot $\langle V_x \rangle$ and $\langle V_y \rangle$ versus F_D in a sample with $\omega = 1.1$, $\phi = 0.49$, and $\tau = 1.4 \times 10^5$ at $F_p = 7$ for varied numbers of pinning sites N_p ranging from $N_p = 50$ to $N_p = 2000$. For this value of ω , a single particle in the absence of pinning moves at the intrinsic Hall angle of $\theta_H^{\text{int}} = \arctan(\omega/\alpha_d) = 53^\circ$ with respect to the driving direction. We find that for $N_p = 50$, the velocity curves increase linearly with F_D , while $\langle V_x \rangle$ and $\langle V_y \rangle$ are close together with $\langle V_y \rangle$ sitting slightly above $\langle V_x \rangle$. As N_p increases, both velocities drop but $\langle V_x \rangle$ decreases more slowly than $\langle V_y \rangle$. At large values of N_p , the velocity-force curves become increasingly nonlinear, similar to what is observed in other driven systems with strong pinning [60]. In Fig. 5, we plot the measured Hall angle $\theta_H = \arctan(\langle V_y \rangle / \langle V_x \rangle)$ versus F_D for the system

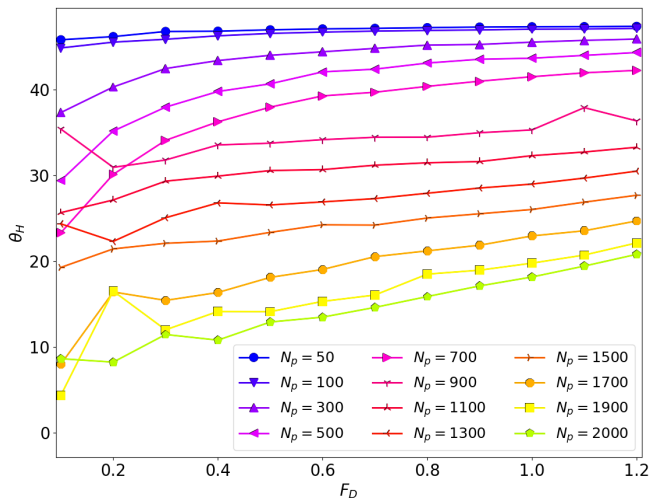


FIG. 5. The measured Hall angle $\theta_H = \arctan(\langle V_y \rangle / \langle V_x \rangle)$ vs F_D for the system from Fig. 4 with $\omega = 1.1$, $\phi = 0.49$, and $\tau = 1.4 \times 10^5$ at $F_p = 7$ for $N_p = 50, 100, 300, 500, 700, 900, 1100, 1300, 1500, 1700, 1900,$ and 2000 , from top to bottom. The Hall angle generally starts off low and increases with increasing drive. In this case, the pin-free value is $\theta_H^{\text{int}} = 53^\circ$.

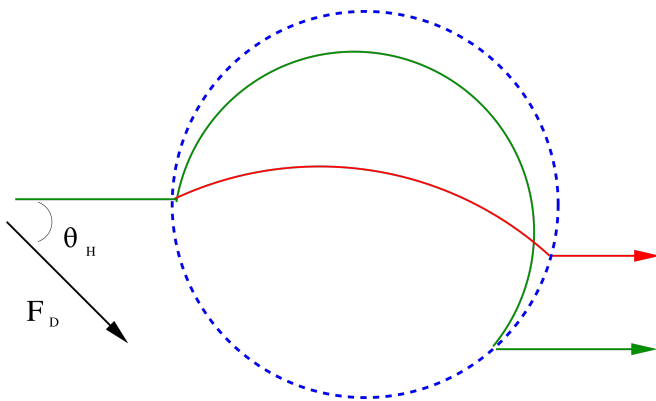


FIG. 6. Schematic showing the motion of a chiral particle through a pinning site (dashed circle), where the frame of reference has been rotated so that the pin-free Hall angle points directly to the right. The driving force F_D (black arrow) is at a downward angle with respect to θ_H^{int} . The green line shows the trajectory for a small driving force, where the Magnus effect on the pinning interaction creates a large side jump toward the direction of the drive, reducing the average Hall angle. The red line is the trajectory of a fast moving particle that spends little time in the pinning site and only experiences a small side jump.

from Fig. 4. When $N_p \leq 100$, θ_H is close to the intrinsic value θ_H^{int} , but for larger values of N_p , θ_H has a low value for low drives and gradually increases with increasing F_D . For example, at $N_p = 700$, $\theta_H \approx 23^\circ$ at the lowest drives and increases up to $\theta_H \approx 40^\circ$ at the highest drives.

The drive dependence of the Hall angle that we find for the chiral disk system is very similar to the drive dependence observed for skyrmions driven over random

pinning arrays. In the skyrmion case, the Hall angle is reduced at low drives because the skyrmion undergoes a side jump every time it passes through a pinning site as a result of the Magnus term [26, 28, 30, 31, 61]. In Fig. 7, we show a schematic of the side jump effect where the frame of reference has been rotated so that the intrinsic Hall angle points directly to the right. When the particle enters the pinning site, it experiences a radial force from the pinning that pushes it toward the center of the pin. The Magnus force rotates this radial force partially into the perpendicular direction, causing the particle to move in an arc. For smaller drives, the particle is shifted downward by a large amount toward the driving direction, and if the particle repeatedly strikes pinning sites as it moves, its average Hall angle is markedly reduced compared to the pin-free value. At high F_D , the size of the side jump diminishes since the amount of time the particle spends interacting with the pinning site is reduced. The results in Fig. 5 indicate that drifting active spinners should also experience a Hall effect and, in the presence of pinning, should show a drive dependent Hall angle similar to that found for skyrmions.

The closest system to what we have studied appears in the work of Lou *et al.* [29], who considered nonactive spinning particles moving through an obstacle array. In that study, the spinning particles had no Hall angle in the absence of obstacles, and a finite Hall angle appeared only when the spinning particles collided with obstacles, which produced a transverse shift in the particle positions. In our case, the Magnus force also acts on the drift force, so there is a finite Hall angle even for zero pinning, while interaction with pinning causes a change in the Hall angle.

In Fig. 7, we replot the $\langle V_x \rangle$ and $\langle V_y \rangle$ versus F_D curves from Fig. 4 on a log-log scale. When $N_p < 1500$, the velocity-force curves are linear over most of their range with $\langle V \rangle \propto F_D$. For these smaller values of N_p , most of the particles continue to move between pinning sites since $N \gg N_p$, and the particles that do become trapped at pins serve as localized drag sites that increase the effective viscosity of the particles flowing around them. For $N_p \geq 1500$, three regimes emerge. At low F_D and high F_D , the velocities increase linearly with the drive, while at intermediate F_D there is a regime in which $\langle V_{x,y} \rangle \propto (F_D)^\alpha$ with $1.5 < \alpha < 2.0$. In previous work on two-dimensional driven systems with strong disorder, a power law dependence of the velocity on the drive was observed with different exponents of $\alpha < 1.0$ for the elastic flow regime and $1.3 < \alpha < 2.0$ in the plastic flow regime [60]. In our system, at low drives the particles that are not trapped directly by the pinning sites undergo interstitial flow past the pinned particles, giving behavior similar to that of fluid flow through a porous medium. At intermediate drives, the pinned particles become only intermittently pinned, leading to plastic flow, while at high drives, all of the particles are continuously moving and the system acts like a fluid again. Figure 5 shows that for $N_p > 1500$, the Hall angle is low and increases linearly

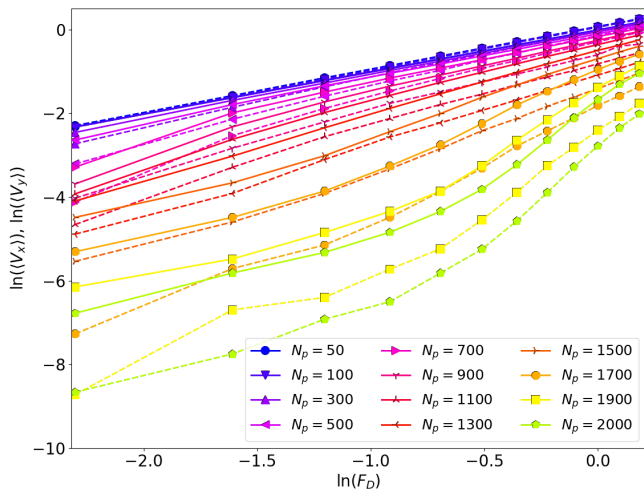


FIG. 7. $\langle V_x \rangle$ (solid lines) and $\langle V_y \rangle$ (dashed lines) vs F_D curves on a log-log scale for the system in Fig. 4 with $\omega = 1.1$, $\phi = 0.49$, and $\tau = 1.4 \times 10^5$ at $F_p = 7$ for $N_p = 50, 100, 300, 500, 700, 900, 1100, 1300, 1500, 1700, 1900,$ and 2000 , from top to bottom. There is a linear increase in the velocity with increasing drive for small values of N_p . For larger values of N_p , the increase becomes non-linear and there is a region where $\langle V_{x,y} \rangle \propto F_D^\alpha$ with exponents of $1.5 < \alpha < 2.0$.

with drive, while for $N_p < 1500$, the increase in the Hall angle is both more rapid and nonlinear. We expect that for $F_D/F_p > 1.0$, θ_H will approach the intrinsic value θ_H^{int} since the particles would be moving so rapidly that they could only interact weakly with the pinning sites.

In Fig. 8(a) we plot $\langle V_x \rangle$ and $\langle V_y \rangle$ versus N_p on a semilog scale for the system from Fig. 7 at $\rho = 0.49$, $\omega = 1.1$, $\tau = 1.4 \times 10^5$, and $F_p = 7.0$ for varied F_D . The velocities decrease with increasing N_p , and the decrease in $\langle V_y \rangle$ is more pronounced than that of $\langle V_x \rangle$. The corresponding plot of θ_H versus N_p in Fig. 8(b) shows that θ_H decreases as the number of pinning sites increases, indicating that there is increased scattering by the pinning sites as N_p becomes larger. Although the θ_H measurements become noisy at low values of F_D , the clear general trend is that the Hall angle decreases with decreasing F_D and increasing N_p .

In Fig. 9(a) we plot $\langle V_x \rangle$ and $\langle V_y \rangle$ at a fixed drive of $F_D = 1.0$ for a sample with $F_p = 7.0$, $N_p = 1100$, $\rho = 0.49$, and $\tau = 1.4 \times 10^5$. As the Magnus strength ω increases, $\langle V_y \rangle$ increases more rapidly than $\langle V_x \rangle$. Figure 9(b) shows the corresponding measured θ_H versus ω along with the expected value θ_H^{int} versus ω for a pin-free system with $N_p = 0$. We find that the Hall angle is always reduced by the pinning, $\theta_H < \theta_H^{\text{int}}$, due to the asymmetric scattering of the particles by the pinning sites.

In Fig. 10 we plot a heat map of the fraction C_L of particles in the largest cluster as a function of F_p versus F_D for a system with $\phi = 0.49$, $\omega = 1.1$, $N_p = 900$, and $\tau = 1.4 \times 10^5$. For low pinning forces, the system is phase separated and C_L is large for all drives. An image of the clustered state obtained for $F_p = 2$ and $F_D = 1.2$ appears

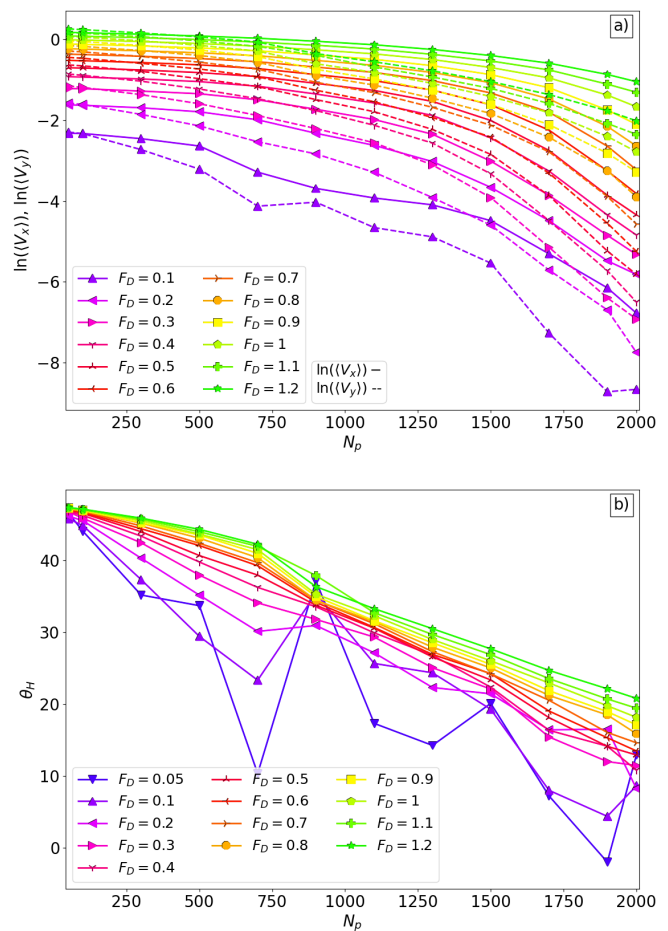


FIG. 8. (a) $\langle V_x \rangle$ (solid lines) and $\langle V_y \rangle$ (dashed lines) vs N_p on a semilog scale for the system from Fig. 4 with $\omega = 1.1$, $\phi = 0.49$, and $\tau = 1.4 \times 10^5$ at $F_p = 7$ for $F_D = 0.1, 0.2, 0.3, 0.4, 0.5, 0.6, 0.7, 0.8, 0.9, 1.0, 1.1,$ and 1.2 from bottom to top. (b) The corresponding θ_H vs N_p curves on a linear scale showing that there is a reduction of the Hall angle with increasing N_p and decreasing F_D .

in Fig. 11(a). The particles in the low density region that have very small velocities have become trapped at pinning sites. Since the system is subjected to a finite drift force, it is more difficult to detect the presence of an edge current using the net displacement measure Δr ; however, an edge current is still present, and the entire cluster acts like an effective macroscopic particle and moves at a Hall angle with respect to the external drive. When F_p is raised to a large value, Fig. 10 indicates that a cluster state appears only for $0 < F_D < 0.2$, as illustrated in Fig. 11(b) for a sample with $F_p = 7$ and $F_D = 0.1$. Here the system forms multiple smaller clusters that are each surrounded by an edge current. As F_D increases at high F_p , C_L drops when the clusters begin to break apart into the plastically flowing state, shown in Fig. 11(c) for a sample with $F_p = 7$ and $F_D = 1.2$. If F_p is lowered to an intermediate value, the clustering persists over a wide drive range but is somewhat suppressed at intermediate

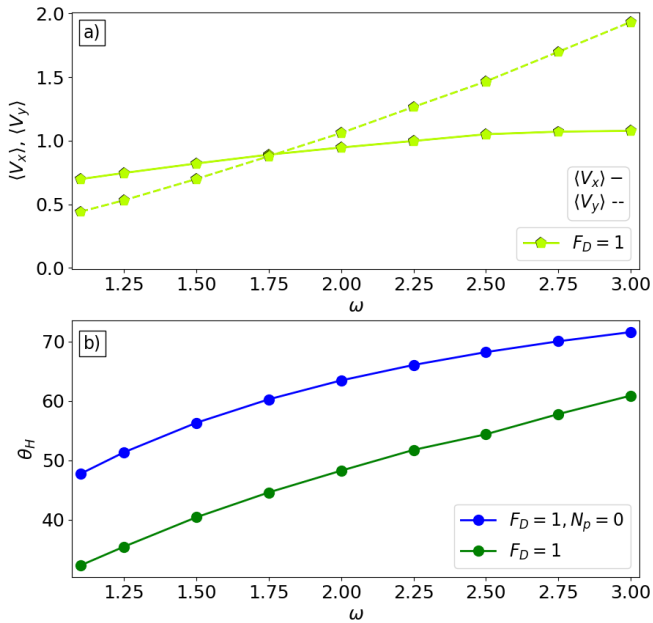


FIG. 9. (a) $\langle V_x \rangle$ (solid line) and $\langle V_y \rangle$ (dashed line) vs Magnus strength ω at a fixed drive of $F_D = 1.0$ for a system with $F_p = 7.0$, $N_p = 1100$, $\rho = 0.49$ and $\tau = 1.4 \times 10^5$. (b) The corresponding θ_H (green) along with the expected value of θ_H^{MF} in a pin-free system (blue) vs ω , both for $F_D = 1$.

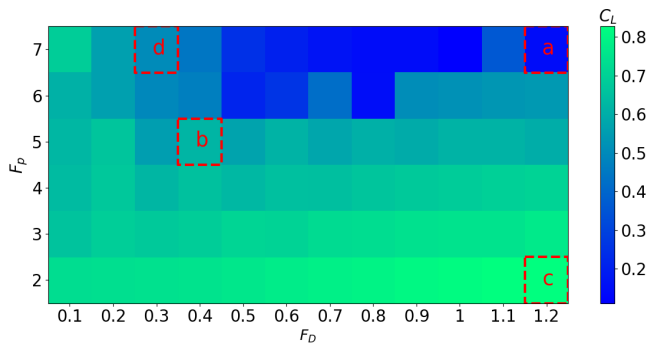


FIG. 10. Heat map of the fraction C_L of particles in the largest cluster as a function of F_p vs F_D for samples with $\phi = 0.49$, $\omega = 1.1$, $N_p = 900$, and $\tau = 1.4 \times 10^5$. The red squares indicate the points at which the images in Fig. 11 were obtained.

drives. Figure 11(d) shows that the system has reformed a cluster for $F_p = 5$ and $F_D = 0.2$; however, the number of pinned particles is substantially higher than in the $F_p = 2$ and $F_D = 1.2$ sample from Fig. 11(a).

The heat map of C_L in Fig. 10 indicates that for low F_D , the system forms a cluster state at high F_p , while for higher F_D , at high F_p the clusters are broken apart by plastic flow. We expect that the system would form a strongly clustered state again even for $F_p = 7.0$ once $F_D > F_p$. We can compare our results to previous simulations performed with $\omega = 0$, where it was also observed that the MIPS cluster state breaks up for strong pinning

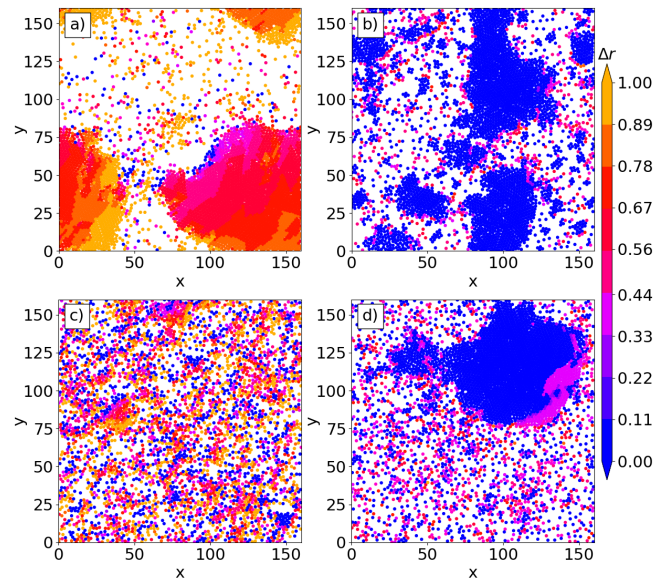


FIG. 11. Images of particle configurations in the system from Fig. 10 at $\phi = 0.49$, $\omega = 1.1$, $N_p = 900$, and $\tau = 1.4 \times 10^5$. Colors indicate the net displacement Δr of the particle during a period of 500 simulation time steps. (a) $F_p = 2$ and $F_D = 1.2$, where there is strong clustering. (b) $F_p = 7$ and $F_D = 0.1$. (c) $F_p = 7$ and $F_D = 1.2$. (d) $F_p = 5$ and $F_D = 0.2$.

at intermediate drive but can reappear at higher drives [12]. This is also consistent with studies in nonactive particles driven over strong quenched disorder, which showed that the system is the most strongly disordered for intermediate drives but can dynamically order at higher drives [60]. Whether or not the system is able to dynamically reorder should also depend on the type of quenched disorder present. For the pinning sites that we consider here, a strong drive causes the particles to move rapidly over the pinning and decouple from it; however, if the pinning sites are replaced by obstacles, the particles remain in a disordered configuration even for very high drives.

IV. NON-ACTIVE CHIRAL DISKS

To examine how general the drive dependence of the Hall effect is, we consider a system in which the particles have a Magnus term but no motor force, $F_m = 0$. In Fig. 12(a) we plot $\langle V_x \rangle$ and $\langle V_y \rangle$ versus F_D for an $F_m = 0$ system with $\phi = 0.49$, $\omega = 1.1$, $F_p = 7.0$, and $N_p = 1100$, the same as one of the samples from Figs. 4 to 9 but with no activity. We find that $\langle V_x \rangle$ increases more rapidly than $\langle V_y \rangle$ with increasing F_D at lower drives. The corresponding plot of θ_H versus F_D in Fig. 12(b) shows that θ_H has a small value at low drives and increases with increasing F_D in a manner similar to that found for the active system in Fig. 5. In Fig. 13(a) we illustrate the particle positions and displacements for the $F_m = 0$ system from Fig. 12 at a drive of $F_D = 0.1$. Most of the

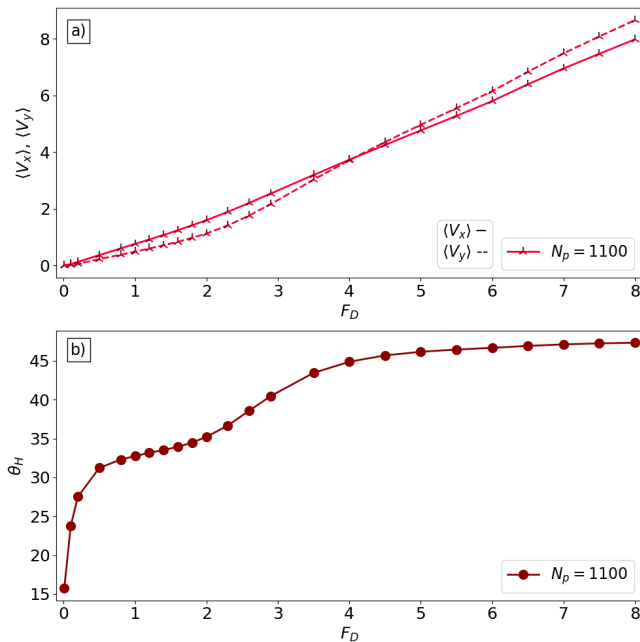


FIG. 12. (a) $\langle V_x \rangle$ (solid line) and $\langle V_y \rangle$ (dashed line) vs F_D for particles with a Magnus term but no activity, $F_m = 0$, in a system with $\phi = 0.49$, $\omega = 1.1$, and $N_p = 1100$. (b) The corresponding Hall angle θ_H vs F_D asymptotically tends toward the pin free value of $\theta_H^{\text{inf}} = 53^\circ$.

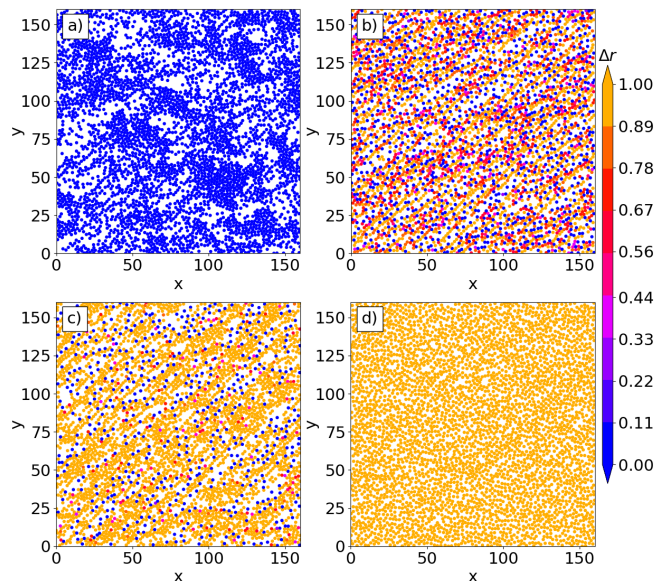


FIG. 13. Images of particle configurations in the system from Fig. 12 with no activity, $F_m = 0$, at $\phi = 0.49$, $\omega = 1.1$, and $N_p = 1100$. Colors indicate the net displacement Δr of the particle during a period of 500 simulation time steps. (a) $F_D = 0.1$. (b) $F_D = 1.5$. (c) $F_D = 3.0$. (d) $F_D = 7.0$.

particles are pinned and we observe the formation of a locally clogged state. At $F_D = 1.5$ in Fig. 13(b), the particles travel at an angle with respect to the direction of the external drive and a wide range of velocity values are present, with some of the particles remaining pinned and other particles moving rapidly through the interstitial regions. Figure 13(c) shows the same system at $F_D = 3.0$ where the velocity distribution has become strongly bimodal, with a smaller set of pinned particles and a large fraction of moving particles all traveling with the same speed. The Hall angle of the motion is larger compared to Fig. 13(b). At $F_D = 7.0$ in Fig. 13(d), $F_D = F_p$ so all of the particles are moving and a disordered uniform state emerges. This result shows that the drive dependence of the Hall angle appears both with and without the active motor force as long as the equations of motion contain a Magnus term.

V. SUMMARY

We have investigated a two-dimensional system of active run-and-tumble particles that have both a damping and a Magnus term in their dynamics. The damping aligns the particle velocities with the net force exerted on the particle, while the Magnus term contributes a velocity component that is perpendicular to the net force. For densities and running times at which the system forms a motility-induced phase separated state (MIPS) in the absence of the Magnus term, we find that inclusion of a Magnus term produces a chiral MIPS phase containing a large rotating cluster with an edge current. The direction of rotation and of the edge current matches the chirality of the Magnus term. As the size of the Magnus term increases, we observe a shear banding effect in which particles along the edges of the cluster form multiple bands moving at different speeds while the center of the cluster rotates as a rigid crystalline solid. We also find that the Magnus term stabilizes the MIPS state down to lower run lengths compared to a Magnus-free system because the Magnus forces push particles on the cluster boundary that would otherwise move radially outward away from the cluster into trajectories that spiral around the edge of the cluster, keeping the particles localized close to the cluster. Similar Magnus-induced clustering effects have been observed in systems of magnetic skyrmions. As the Magnus term increases, the shear bands increase in width and destroy the crystalline order of the cluster center, and when the Magnus force becomes dominant, the phase separation is lost and a chiral labyrinthine state emerges.

We examined the effect of including quenched disorder and a uniform drift force. Without quenched disorder, the rotating MIPS cluster moves at a Hall angle with respect to the applied drift force that is determined by the ratio of the Magnus term to the damping term. When quenched disorder is present, nonlinearity appears in the velocity-force curves and the Hall angle becomes

drive dependent, taking a small value at low drives and asymptotically approaching the intrinsic or pin-free value as the drive increases. This is the result of the side jump, experienced by the particles as they move through the pinning sites, that becomes smaller as the drive becomes larger. The velocity dependent Hall angle is the same effect observed for magnetic skyrmions, which have a Magnus term in their dynamics, driven over quenched disorder. We find that even when the quenched disorder is very strong, the particles still form a cluster or phase-separated state at zero drive, but at finite drives, plastic events produced by the interaction between pinned and moving interstitial particles tear the clusters apart; however, at large drives, the clusters can reform. The velocity dependence of the Hall angle persists even when the motor force is shut off so that there is no run-and-tumble

component to the particle motion.

ACKNOWLEDGMENTS

We gratefully acknowledge the support of the U.S. Department of Energy through the LANL/LDRD program for this work. This work was supported by the US Department of Energy through the Los Alamos National Laboratory. Los Alamos National Laboratory is operated by Triad National Security, LLC, for the National Nuclear Security Administration of the U. S. Department of Energy (Contract No. 892333218NCA000001). AL was supported by a grant of the Romanian Ministry of Education and Research, CNCS - UEFISCDI, project number PN-III-P4-ID-PCE-2020-1301, within PNC DI III.

-
- [1] M. C. Marchetti, J. F. Joanny, S. Ramaswamy, T. B. Liverpool, J. Prost, M. Rao, and R. A. Simha, “Hydrodynamics of soft active matter,” *Rev. Mod. Phys.* **85**, 1143–1189 (2013).
- [2] Y. Fily and M. C. Marchetti, “Athermal phase separation of self-propelled particles with no alignment,” *Phys. Rev. Lett.* **108**, 235702 (2012).
- [3] G. S. Redner, M. F. Hagan, and A. Baskaran, “Structure and dynamics of a phase-separating active colloidal fluid,” *Phys. Rev. Lett.* **110**, 055701 (2013).
- [4] J. Palacci, S. Sacanna, A. P. Steinberg, D. J. Pine, and P. M. Chaikin, “Living crystals of light-activated colloidal surfers,” *Science* **339**, 936–940 (2013).
- [5] I. Buttinoni, J. Biaké, F. Kümmel, H. Löwen, C. Bechinger, and T. Speck, “Dynamical clustering and phase separation in suspensions of self-propelled colloidal particles,” *Phys. Rev. Lett.* **110**, 238301 (2013).
- [6] M. E. Cates and J. Tailleur, “Motility-induced phase separation,” *Ann. Rev. Cond. Mat. Phys.* **6**, 219–244 (2015).
- [7] C. Reichhardt and C. J. Olson Reichhardt, “Absorbing phase transitions and dynamic freezing in running active matter systems,” *Soft Matter* **10**, 7502–7510 (2014).
- [8] O. Chepizhko, E. G. Altmann, and F. Peruani, “Optimal noise maximizes collective motion in heterogeneous media,” *Phys. Rev. Lett.* **110**, 238101 (2013).
- [9] A. Morin, N. Desreumaux, J.-B. Caussin, and D. Bartolo, “Distortion and destruction of colloidal flocks in disordered environments,” *Nature Phys.* **13**, 63–67 (2017).
- [10] Cs. Sándor, A. Libál, C. Reichhardt, and C. J. Olson Reichhardt, “Dewetting and spreading transitions for active matter on random pinning substrates,” *J. Chem. Phys.* **146**, 204903 (2017).
- [11] D. Yllanes, M. Leoni, and M. C. Marchetti, “How many dissenters does it take to disorder a flock?” *New J. Phys.* **19**, 103026 (2017).
- [12] Cs. Sándor, A. Libál, C. Reichhardt, and C. J. Olson Reichhardt, “Dynamic phases of active matter systems with quenched disorder,” *Phys. Rev. E* **95**, 032606 (2017).
- [13] A. Chardac, S. Shankar, M. C. Marchetti, and D. Bartolo, “Emergence of dynamic vortex glasses in disordered polar active fluids,” *Proc. Natl. Acad. Sci. (USA)* **118**, e2018218118 (2021).
- [14] T. Bhattacharjee and S. S. Dutta, “Bacterial hopping and trapping in porous media,” *Nature Commun.* **10**, 2075 (2019).
- [15] S. Shi, H. Li, G. Feng, W. Tian, and K. Chen, “Transport of self-propelled particles across a porous medium: trapping, clogging, and the Matthew effect,” *Phys. Chem. Chem. Phys.* **22**, 14052 (2020).
- [16] C. Reichhardt and C. J. Olson Reichhardt, “Active matter transport and jamming on disordered landscapes,” *Phys. Rev. E* **90**, 012701 (2014).
- [17] H. Aref, J. B. Kadtke, I. Zawadzki, L. J. Campbell, and B. Eckhardt, “Point vortex dynamics: recent results and open problems,” *Fluid Dynam. Res.* **3**, 63–74 (1988).
- [18] C. Reichhardt and C. J. O. Reichhardt, “Dynamics of Magnus-dominated particle clusters, collisions, pinning, and ratchets,” *Phys. Rev. E* **101**, 062602 (2020).
- [19] V. Novosad, F. Y. Fradin, P. E. Roy, K. S. Buchanan, K. Yu. Guslienko, and S. D. Bader, “Magnetic vortex resonance in patterned ferromagnetic dots,” *Phys. Rev. B* **72**, 024455 (2005).
- [20] A. Melzer, H. Krüger, D. Maier, and S. Schütt, “Physics of magnetized dusty plasmas,” *Rev. Mod. Plasma Phys.* **5**, 11 (2021).
- [21] R. Shinde, J. U. Sommer, H. Löwen, and A. Sharma, “Strongly enhanced dynamics of a charged Rouse dimer by an external magnetic field,” *PNAS Nexus* **1**, pgac119 (2022).
- [22] D. Doshi and A. Gromov, “Vortices as fractons,” *Commun. Phys.* **4**, 44 (2021).
- [23] S. Mühlbauer, B. Binz, F. Jonietz, C. Pfleiderer, A. Rosch, A. Neubauer, R. Georgii, and P. Böni, “Skyrmion lattice in a chiral magnet,” *Science* **323**, 915–919 (2009).
- [24] N. Nagaosa and Y. Tokura, “Topological properties and dynamics of magnetic skyrmions,” *Nature Nanotechnol.* **8**, 899–911 (2013).
- [25] K. Everschor-Sitte and M. Sitte, “Real-space Berry phases: Skyrmion soccer (invited),” *J. Appl. Phys.* **115**, 172602 (2014).
- [26] C. Reichhardt, C. J. O. Reichhardt, and M. Milošević, “Statics and dynamics of skyrmions interacting with disorder and nanostructures,” *Rev. Mod. Phys.* **94**, 035005 (2022).

- (2022).
- [27] E. H. Hall, “On a new action of the magnet on electric currents,” *Am. J. Math.* **2**, 287–292 (1879).
- [28] C. Reichhardt, D. Ray, and C. J. Olson Reichhardt, “Collective transport properties of driven skyrmions with random disorder,” *Phys. Rev. Lett.* **114**, 217202 (2015).
- [29] X. Lou, Q. Yang, Y. Ding, P. Liu, K. Chen, X. Zhou, F. Ye, R. Podgornik, and M. Yang, “Odd viscosity-induced hall-like transport of an active chiral fluid,” *Proc. Natl. Acad. Sci. (USA)* **119**, e2201279119 (2022).
- [30] W. Jiang, X. Zhang, G. Yu, W. Zhang, X. Wang, M. B. Jungfleisch, J. E. Pearson, X. Cheng, O. Heinonen, K. L. Wang, Y. Zhou, A. Hoffmann, and S. G. E. te Velthuis, “Direct observation of the skyrmion Hall effect,” *Nature Phys.* **13**, 162–169 (2017).
- [31] K. Litzius, I. Lemesh, B. Krüger, P. Bassirian, L. Caretta, K. Richter, F. Büttner, K. Sato, O. A. Tretiakov, J. Förster, R. M. Reeve, M. Weigand, I. Bykova, H. Stoll, G. Schütz, G. S. D. Beach, and M. Kläui, “Skyrmion Hall effect revealed by direct time-resolved X-ray microscopy,” *Nature Phys.* **13**, 170–175 (2017).
- [32] F. Kümmel, B. ten Hagen, R. Wittkowski, I. Buttinoni, R. Eichhorn, G. Volpe, H. Löwen, and C. Bechinger, “Circular motion of asymmetric self-propelling particles,” *Phys. Rev. Lett.* **110**, 198302 (2013).
- [33] L. Lemelle, J.-F. Paliarne, E. Chatre, and C. Place, “Counterclockwise circular motion of bacteria swimming at the air-liquid interface,” *J. Bacteriol.* **192**, 6307–6308 (2010).
- [34] A. Nourhani, V. H. Crespi, and P. E. Lammert, “Guiding chiral self-propellers in a periodic potential,” *Phys. Rev. Lett.* **115**, 118101 (2015).
- [35] H. Löwen, “Chirality in microswimmer motion: From circle swimmers to active turbulence,” *Eur. Phys. J. Spec. Top.* **225**, 2319–2331 (2016).
- [36] M. Han, J. Yan, S. Granick, and E. Luijten, “Effective temperature concept evaluated in an active colloid mixture,” *Proc. Natl. Acad. Sci. (USA)* **114**, 7513–7518 (2017).
- [37] B. Liebchen and D. Levis, “Chiral active matter,” *EPL* **139**, 67001 (2022).
- [38] B. C. van Zuiden, J. Paulose, W. T. M. Irvine, D. Bartolo, and V. Vitelli, “Spatiotemporal order and emergent edge currents in active spinner materials,” *Proc. Natl. Acad. Sci. (USA)* **113**, 12919–12924 (2016).
- [39] D. Banerjee, A. Souslov, A. G. Abanov, and V. Vitelli, “Odd viscosity in chiral active fluids,” *Nature Commun.* **8**, 1573 (2017).
- [40] K. Dasbiswas, K. K. Mandadapu, and S. Vaikuntanathan, “Topological localization in out-of-equilibrium dissipative systems,” *Proc. Natl. Acad. Sci. (USA)* **115**, E9031–E9040 (2018).
- [41] V. Soni, E. S. Bililign, S. Magkiriadou, S. Sacanna, D. Bartolo, M. J. Shelley, and W. T. M. Irvine, “The odd free surface flows of a colloidal chiral fluid,” *Nature Phys.* **15**, 1188 (2019).
- [42] C. Reichhardt and C. J. O. Reichhardt, “Reversibility, pattern formation, and edge transport in active chiral and passive disk mixtures,” *J. Chem. Phys.* **150**, 064905 (2019).
- [43] X. Yang, C. Ren, K. Cheng, and H. P. Zhang, “Robust boundary flow in chiral active fluid,” *Phys. Rev. E* **101**, 022603 (2020).
- [44] M. Han, M. Fruchart, C. Scheibner, S. Vaikuntanathan, J. J. de Pablo, and V. Vitelli, “Fluctuating hydrodynamics of chiral active fluids,” *Nature Phys.* **17**, 1260–1269 (2021).
- [45] M. Fruchart, C. Scheibner, and V. Vitelli, “Odd viscosity and odd elasticity,” *Ann. Rev. Condens. Matter Phys.* **14**, 471–510 (2023).
- [46] A. P. Petroff, C. Whittington, and A. Kudrolli, “Density-mediated spin correlations drive edge-to-bulk flow transition in active chiral matter,” *Phys. Rev. E* **108**, 014609 (2023).
- [47] E. Kalz, H. D. Vuijk, I. Abdoli, J.-U. Sommer, H. Löwen, and A. Sharma, “Collisions enhance self-diffusion in odd-diffusive systems,” *Phys. Rev. Lett.* **129**, 090601 (2022).
- [48] X. Cao, D. Das, N. Windbacher, F. Ginot, M. Krüger, and C. Bechinger, “Memory-induced Magnus effect,” *Nature Phys.*, in press (2023).
- [49] C. Reichhardt and C. J. O. Reichhardt, “Active microrheology, Hall effect, and jamming in chiral fluids,” *Phys. Rev. E* **100**, 012604 (2019).
- [50] C. J. O. Reichhardt and C. Reichhardt, “Active rheology in odd-viscosity systems,” *EPL* **137**, 66004 (2022).
- [51] A. R. Poggioli and D. T. Limmer, “Odd mobility of a passive tracer in a chiral active fluid,” *Phys. Rev. Lett.* **130**, 158201 (2023).
- [52] N. H. P. Nguyen, D. Klotsa, M. Engel, and S. C. Glotzer, “Emergent collective phenomena in a mixture of hard shapes through active rotation,” *Phys. Rev. Lett.* **112**, 075701 (2014).
- [53] A. Aubret, M. Youssef, S. Sacanna, and J. Palacci, “Targeted assembly and synchronization of self-spinning microgears,” *Nature Phys.* **14**, 1114–1118 (2018).
- [54] T. H. Tan, A. Mietke, J. Li, Y. Chen, H. Higinbotham, P. J. Foster, S. Gokhale, J. Dunkel, and N. Fakhri, “Odd dynamics of living chiral crystals,” *Nature* **607**, 287–293 (2022).
- [55] W. R. DiLuzio, L. Turner, M. Mayer, P. Garstecki, D. B. Weibel, H. C. Berg, and G. M. Whitesides, “*Escherichia coli* swim on the right-hand side,” *Nature (London)* **435**, 1271–1274 (2005).
- [56] H. Wioland, F. G. Woodhouse, J. Dunkel, and R. E. Goldstein, “Ferromagnetic and antiferromagnetic order in bacterial vortex lattices,” *Nature Phys.* **12**, 341 (2016).
- [57] H. Reinken, D. Nishiguchi, S. Heidenreich, A. Sokolov, M. Bär, S. H. L. Klapp, and I. S. Aranson, “Organizing bacterial vortex lattices by periodic obstacle arrays,” *Commun. Phys.* **3**, 76 (2020).
- [58] S. Luding and H. J. Herrmann, “Cluster-growth in freely cooling granular media,” *Chaos* **9**, 673–681 (1999).
- [59] C. Bechinger, R. Di Leonardo, H. Löwen, C. Reichhardt, G. Volpe, and G. Volpe, “Active particles in complex and crowded environments,” *Rev. Mod. Phys.* **88**, 045006 (2016).
- [60] C. Reichhardt and C. J. Olson Reichhardt, “Depinning and nonequilibrium dynamic phases of particle assemblies driven over random and ordered substrates: a review,” *Rep. Prog. Phys.* **80**, 026501 (2017).
- [61] I. L. Fernandes, J. Chico, and S. Lounis, “Impurity-dependent gyrotropic motion, deflection and pinning of current-driven ultrasmall skyrmions in PdFe/Ir(111) surface,” *J. Phys.: Condens. Matter* **32**, 425802 (2020).